Engineering 16 (2022) 100–114

Contents lists available at ScienceDirect

Engineering

journal homepage: www.elsevier.com/locate/eng

Research
Reconfigurable Antennas—Article

A Polarization Programmable Antenna Array

Dingzhao Chen [a,c], Yanhui Liu [b,c,*], Ming Li [c,d], Pan Guo [b], Zhuo Zeng [a], Jun Hu [b], Y. Jay Guo [d,*]

[a] Institute of Electromagnetics and Acoustics, Xiamen University, Xiamen 361000, China
[b] School of Electronic Science and Engineering, University of Electronic Science and Technology of China, Chengdu 611731, China
[c] Yangtze Delta Region Institute (Quzhou), University of Electronic Science and Technology of China, Quzhou 324000, China
[d] Global Big Data Technologies Centre, University of Technology Sydney (UTS), NSW 2007, Australia

ARTICLE INFO

Article history:
Received 3 September 2021
Revised 6 January 2022
Accepted 27 March 2022
Available online 6 May 2022

Keywords:
Antenna array
Polarization reprogrammable antenna
Reconfigurable antenna

ABSTRACT

Reconfigurable antennas are becoming a major antenna technology for future wireless communications and sensing systems. It is known that, with a single linear polarization (LP) reconfigurable antenna element, a preferred polarization can be produced from a set of multiple polarization states, thus improving the quality of the communication link. This paper presents a new concept of a polarization programmable reconfigurable antenna array that consists of a number of polarization reconfigurable antenna elements with a finite number of possible polarization states. By employing a new optimization strategy and programming the polarization states of all the array elements, we demonstrate that it is possible to realize any desired LP in the vectorial array radiation pattern with accurate control of sidelobe and cross-polarization levels (XPLs), thereby achieving the desired polarization to perfectly match that of the required communications signal. Both numerical and experimental results are provided to prove the concept, and they agree well with each other.

1. Introduction

Conventional antennas are designed according to given system specifications, which include the beam pattern, antenna gain, sidelobe level (SLL), and polarization. To meet the demand of various advanced communications systems and multifunctional platforms, there has been fast-growing research interest and technology development in reconfigurable antennas in recent years [1,2]. By employing switching and tuning devices, as well as advanced materials, reconfigurable antennas can change the antenna characteristics on the fly to meet the system requirements in real time. Reconfigurable antennas can be classified as pattern reconfigurable antennas, frequency reconfigurable antennas, and polarization reconfigurable antennas [3–5]. To date, the majority of reported reconfigurable antennas are in the form of single antenna elements.

For a receive system, employing reconfigurable antennas with multi-polarization ability can effectively reduce polarization mismatch. A number of antennas are presented in Refs. [6–15] with the ability of reconfigurability among two orthogonal circular polarizations (CPs) and two orthogonal linear polarizations (LPs). However, when these antennas are utilized to receive an arbitrary LP signal, they may still suffer as much as 50% polarization mismatch losses. Thus, to improve the signal quality when receiving arbitrary LP waves, various multi-LP reconfigurable (MLPR) antennas are proposed in Refs. [16–25]. Generally speaking, MLPR antennas can be subdivided into two categories: radiator reconfigurable antennas [16–20] and feed network reconfigurable antennas [21–25]. By loading radio frequency (RF) switches, such as positive–intrinsic–negative (PIN) diodes, to a reconfigurable structure, the polarization of the antenna can be controlled by configuring the On–Off states of the switches.

In most practical systems, high antenna gain and a certain degree of beam control are required, so antenna arrays are typically employed. To the best of our knowledge, only a few studies have been published on multi-polarization antenna arrays [26–32]. In Ref. [26], an array with rotatable antenna elements and phase shifters is proposed, which can change the polarization ellipticity of the radiated wave. In Ref. [27], a uniform crossed-dipole array is designed to receive the RF signal in two orthogonal components. The antenna array can be used to estimate the direction of arrival and the polarization of incident waves. However, the

* Corresponding authors.
E-mail addresses: yhliu@uestc.edu.cn (Y. Liu), Jay.Guo@uts.edu.au (Y.J. Guo).

https://doi.org/10.1016/j.eng.2022.03.015

techniques reported in Refs. [26,27] require complex amplitude and phase-control networks; moreover, they are only theoretical and are not validated using actual arrays. In Ref. [28], two polarization-agile active microstrip patch antenna arrays with three elements are designed. The adopted element antenna is loaded with transistors to achieve CP states and LP states. However, the cross-polarization level (XPL) of the proposed arrays tends to be higher than −12 dB. In Ref. [31], a 1 × 4 reconfigurable aperture-fed patch antenna array is reported. By loading controllable RF switches on the cross-aperture, the array achieves ±45° LP reconfigurability. However, its XPL is −10 dB. In addition, SLL is an important figure of merit for antenna arrays. Reducing the SLL of an array pattern can enhance the anti-interference ability of the antenna array. Many studies have reported optimizing the amplitude, phase, and position of array elements through various methods to achieve SLL reduction [33–36]. These include, for example, genetic algorithm (GA) [33], particle swarm optimization (PSO) [34], fast Fourier transform (FFT) [35], and convex (CVX) optimization techniques [36]. However, these arrays usually require unequal power dividers, which increase the complexity and difficulty of the array design. Subsequently, in Ref. [37], the orientations of the dipole elements in an array are optimized to reduce the SLL with a constrained XPL. Using this technique, a reduced SLL pattern can be generated without employing unequal power dividers. In Ref. [38], this technique is further developed to reduce the SLL by appropriately choosing the element orientation from a set of discrete angles. In Refs. [39–41], the polarization orientation of the element antenna is implemented as an optimization variable for array beam control. However, these studies only focus on beamforming at a certain fixed polarization using rotated single-polarized elements. The arrays proposed in the above studies lack the ability to realize polarization reconfigurability while generating an SLL reduction pattern.

In this paper, we propose a new concept of a polarization programmable antenna array that employs multi-LP elements. The array is composed of a number of polarization reconfigurable antenna elements with a finite number of possible polarization states. By employing a new optimization strategy and programming the polarization states of all the array elements, we demonstrate that it is possible to realize any desired LP in the vectorial array radiation pattern with accurate control of the SLL and XPL, thereby achieving the desired polarization to perfectly match that of the required communication signal while employing equal power dividers. To validate the proposed concept, a prototype array of 16 antenna elements, each having eight possible polarization states, was designed and fabricated. The reconfigurable array, which is controlled by a field programmable gate array (FPGA) board for real-time operation, achieves an SLL and XPL lower than −16 dB for different desired LPs, thus validating the proposed technique and method. The overlapped impedance bandwidth is 8.6% and covers 4.77–5.20 GHz, while the peak gain of the array under optimized polarization state configurations is 17.34–17.53 dBi. To the best of our knowledge, this is the first time such an antenna array has been reported.

2. Antenna array system model and optimization strategy

In this section, we present the antenna array model first and then describe the strategy for polarization state optimization. The latter involves the optimization of the element polarization states and employment of a binary GA (BGA) to achieve a pattern with the desired SLL and XPL for any chosen LP.

2.1. The MLPR antenna array

Consider a linear array consisting of N MLPR antenna elements that can be reconfigured independently among M states, as shown in Fig. 1. There are M^N possible polarization states in total for this array. The antenna elements are uniformly arranged along the x-axis, and the element spacing is d. The array elements are fed with the same amplitudes by equal power dividers, and the polarization state of each antenna element is controlled by an FPGA. For the nth element in the array, we use a binary number $P_{n,m}$ to represent the switching state of its mth polarization state, where $P_{n,m}$ = 1 means switching to the On state and $P_{n,m}$ = 0 means switching to the Off state of the mth polarization of the nth element. Clearly, when the mth polarization of the nth element is switched On, all other polarization states would be switched Off for this element. In other words, each element can have only one state. Thus, considering the mutual coupling effect, the array pattern can be described as follows:

$$\boldsymbol{F}(\theta,\phi)=\sum_{n=1}^{N}\sum_{m=1}^{M}P_{n,m}\cdot\boldsymbol{E}_n(\theta,\phi;m)\cdot e^{j\beta x_n\cos\phi\sin\theta}$$

$$P_{n,m}=\begin{cases}1 & \text{if } n\text{th element is in } m\text{th polarization state}\\ 0 & \text{others}\end{cases} \tag{1}$$

$$\sum_{m=1}^{M}P_{n,m}=1\quad \text{for } n=1,2,\ldots,N$$

where j is an imaging number and $j=\sqrt{-1}$; θ is the elevation angle from the positive z-axis; ϕ is the azimuth angle from the positive x-axis; β is the wavenumber in free space; x_n is the position of the nth element; and $\boldsymbol{E}_n(\theta,\phi;m)$ is the vectorial active element pattern (VAEP) of the nth element in its mth polarization state. Once a polarization state configuration of the array is selected, the array pattern can be obtained. The polarization state configuration of the array can be represented by a vector $\boldsymbol{S}_{1\times N}=[s_1,\ldots,s_n,\ldots,s_N]$, where $s_n=\sum_{m=1}^{M}P_{n,m}\cdot m$ is defined as the polarization state value of the nth element. Thus, for an array with an $\boldsymbol{S}_{1\times N}$ polarization state configuration, its vectorial radiation pattern can be written as follows:

$$\boldsymbol{F}(\theta,\phi;\boldsymbol{S}_{1\times N})=\sum_{n=1}^{N}\boldsymbol{E}_n(\theta,\phi;\boldsymbol{S}_{1\times N})\cdot e^{j\beta x_n\cos\phi\sin\theta} \tag{2}$$

where $\boldsymbol{E}_n(\theta,\phi;\boldsymbol{S}_{1\times N})$ is the VAEP of the nth element, which is obtained under the $\boldsymbol{S}_{1\times N}$ polarization state configuration.

It is known that the VAEP of the nth element can be decomposed into the unit vectors $\boldsymbol{e}_\theta$ and $\boldsymbol{e}_\phi$ components:

$$\boldsymbol{E}_n(\theta,\phi;\boldsymbol{S}_{1\times N})=E_{n,\theta}(\theta,\phi;\boldsymbol{S}_{1\times N})\cdot\boldsymbol{e}_\theta+E_{n,\phi}(\theta,\phi;\boldsymbol{S}_{1\times N})\cdot\boldsymbol{e}_\phi \tag{3}$$

Thus, we obtain the following:

$$\begin{cases}\boldsymbol{F}_\theta(\theta,\phi;\boldsymbol{S}_{1\times N})=\sum_{n=1}^{N}\boldsymbol{E}_{n,\theta}(\theta,\phi;\boldsymbol{S}_{1\times N})\cdot e^{j\beta x_n\cos\phi\sin\theta}\\ \boldsymbol{F}_\phi(\theta,\phi;\boldsymbol{S}_{1\times N})=\sum_{n=1}^{N}\boldsymbol{E}_{n,\phi}(\theta,\phi;\boldsymbol{S}_{1\times N})\cdot e^{j\beta x_n\cos\phi\sin\theta}\end{cases} \tag{4}$$

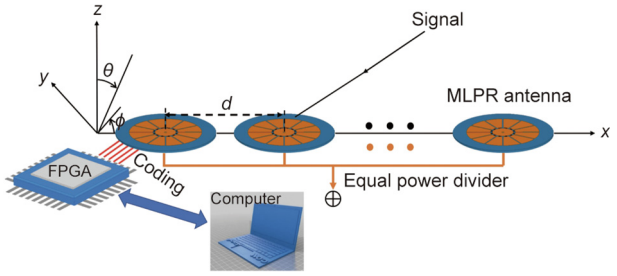

Fig. 1. Illustration of a polarization programmable antenna array. θ: the elevation angle from the positive z-axis; ϕ: the azimuth angle from the positive x-axis; d: the element spacing.

Ideally, for the MLPR antenna array, it is desirable to generate radiation with any desired LP $\boldsymbol{P}_{\mathrm{d}}$ and with the SLL and XPL controlled. However, one problem is that $\boldsymbol{P}_{\mathrm{d}}$ is usually given as a fixed unit vector to indicate direction. $\boldsymbol{P}_{\mathrm{d}}$ can be denoted as $(\vartheta_{\mathrm{d}}, \varphi_{\mathrm{d}})$, where ϑ_{d} and φ_{d} represent its elevation and azimuth, respectively. For the array placed on the *xy*-plane, here we only consider the case in which $\boldsymbol{P}_{\mathrm{d}}$ is parallel to the *xy*-plane—that is, $\vartheta_{\mathrm{d}} = 90°$. As shown in Fig. 2, the transmitting antenna is located at the origin of the rectangular coordinates, and φ_{d} denotes the angle between $\boldsymbol{P}_{\mathrm{d}}$ and $\boldsymbol{e}_x$. The initial position of the probe antenna is at $\theta = 0°$. To measure the co-polarization (CoP) pattern of the antenna, the probe antenna is rotated about its axis to make its polarization parallel to the desired polarization direction. The probe antenna then moves around the transmitting antenna. It should be noted that, as the probe antenna moves, it remains fixed about its axis and always points toward the origin of the coordinates. Thus, the probe antenna remains in the same relative orientation to the unit vectors $\boldsymbol{e}_\theta$ and $\boldsymbol{e}_\phi$. Then, the polarization of the probe antenna ($\boldsymbol{P}_{\mathrm{a}}$) can be written as:

$$\boldsymbol{P}_{\mathrm{a}}(\theta,\phi) = \boldsymbol{e}_\theta \cos(\varphi_{\mathrm{d}} - \phi) + \boldsymbol{e}_\phi \sin(\varphi_{\mathrm{d}} - \phi) \tag{5}$$

Therefore, the realized or measured CoP pattern can be obtained as follows:

$$\begin{aligned}\boldsymbol{F}_{\mathrm{co}}(\theta,\phi;\boldsymbol{S}_{1\times N}) &= (\boldsymbol{F}(\theta,\phi;\boldsymbol{S}_{1\times N})\cdot\boldsymbol{P}_{\mathrm{a}}(\theta,\phi))\cdot\boldsymbol{P}_{\mathrm{a}}(\theta,\phi)\\ &= \boldsymbol{F}_\theta(\theta,\phi;\boldsymbol{S}_{1\times N})\cdot\cos(\varphi_{\mathrm{d}} - \phi) + \boldsymbol{F}_\phi(\theta,\phi;\boldsymbol{S}_{1\times N})\cdot\\ &\quad \sin(\varphi_{\mathrm{d}} - \phi)\end{aligned} \tag{6}$$

When testing the cross-polarization (XP) pattern, the polarization of the probe antenna at $\theta = 0°$ is orthogonal to $\boldsymbol{P}_{\mathrm{d}}$. Then, the XP pattern is obtained by the following:

$$\begin{aligned}\boldsymbol{F}_{\mathrm{X}}(\theta,\phi;\boldsymbol{S}_{1\times N}) = &-\boldsymbol{F}_\theta(\theta,\phi;\boldsymbol{S}_{1\times N})\cdot\sin(\varphi_{\mathrm{d}} - \phi) + \boldsymbol{F}_\phi(\theta,\phi;\boldsymbol{S}_{1\times N})\cdot\\ &\cos(\varphi_{\mathrm{d}} - \phi)\end{aligned} \tag{7}$$

The definition of the CoP and XP components, which is proposed in Ref. [42], is known as Ludwig's definitionIII. With this definition, once the $\boldsymbol{e}_\theta$ and $\boldsymbol{e}_\phi$ components of the vectorial array patterns are obtained, the realized CoP and XP array patterns in the $\boldsymbol{P}_{\mathrm{d}}$ can be calculated.

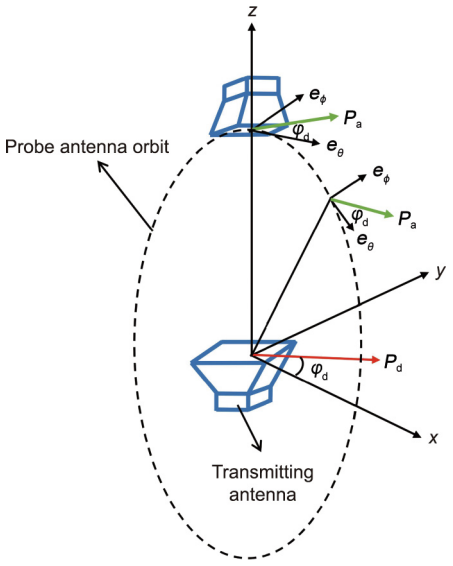

Fig. 2. Schematic diagram of measuring the CoP pattern of the antenna. $\boldsymbol{P}_{\mathrm{a}}$: the polarization of probe antenna.

The main problem here is to generate the desired radiation in any desired LP by optimizing the array polarization state configuration $\boldsymbol{S}_{1\times N} = [s_1, \ldots, s_n, \ldots, s_N]$. From Eqs. (6) and (7), when all the element polarization states s_n satisfy $\varphi_n = \varphi_{\mathrm{d}}$ for n = 1, 2, …, N, where φ_n is the azimuth angle of s_n, the MLPR antenna array can generate radiation in the desired polarization. However, in this way, the array can generate only a few discrete polarizations and usually has an SLL of −13.5 dB.

To generate radiation in any desired LP with a reduced SLL, we can choose to optimize the array polarization state configuration $\boldsymbol{S}_{1\times N}$. To this end, an appropriate fitness function can be used in the optimization process. Suppose that the desired SLL and XPL are denoted as Γ_{SLL} and Γ_{XPL}, respectively. The fitness function can be defined as follows:

$$f = \frac{W_1}{A}\sum_{a=1}^{A}\frac{1}{2}(X_a + |X_a|)^2 + \frac{W_2}{B}\sum_{b=1}^{B}\frac{1}{2}(Y_b + |Y_b|)^2 \tag{8}$$

where

$$\begin{cases} X_a = |\boldsymbol{F}_{\mathrm{co}}(\theta_a,\phi;\boldsymbol{S}_{1\times N})|^2 - \Gamma_{\mathrm{SLL}};\theta_a \in \text{SLL region} \\ Y_b = |\boldsymbol{F}_{\mathrm{X}}(\theta_b,\phi;\boldsymbol{S}_{1\times N})|^2 - \Gamma_{\mathrm{XPL}};\theta_b \in \text{XPL region} \end{cases} \tag{9}$$

and where W_1 and W_2 are user-defined weighting factors. Here, θ_a for a = 1, 2, …, A are the sampling angles in the sidelobe region, and θ_b for b = 1, 2, …, B are the sampling angles in the region where the XPL needs to be controlled. The fitness function in Eq. (8) is to be minimized so that a pattern with a desired LP and constrained SLL and XPL can be obtained.

In order to calculate the array radiation pattern with mutual coupling, it is necessary to obtain the VAEP of each element. In principle, VAEPs can be acquired by full-wave electromagnetic simulations. However, the VAEP of one element antenna is not only related to its own polarization state but also affected by the polarization states of its neighboring elements in the array environment, due to the mutual coupling effect. Therefore, in order to use the polarization state selection method to achieve the desired array pattern, it is necessary to obtain the VAEP of each element in different polarization states under various array polarization configurations. A total number of M^N coupled element patterns need to be obtained. For example, if the array has 16 elements and each element can be reconfigurable among eight polarization states (i.e., N = 16 and M = 8), then a total number of 8^{16} VAEPs need to be obtained. This is not feasible in practice. Therefore, for the purpose of optimizing the element polarization states of the MLPR antenna array, a good approximate method must be adopted to obtain the VAEPs of the elements in different state configurations.

2.2. Pattern approximation for an array with MLPR antenna elements

To obtain the VAEPs of the array elements in the optimization process, we assume that the mutual coupling variation due to the change in the element polarization states does not affect the VAEPs very much. This assumption is generally valid if the changes introduced in each step of the array polarization state optimization are small. Thus, the pattern of an element is mainly affected by the change of its own polarization state. In this situation, if we choose a symmetrical structure for the MLPR antenna element, switching one polarization state of the antenna element to another can be regarded as a rotation of the antenna. Hence, obtaining the VAEPs of one element in each polarization state can be accomplished by mathematically rotating the VAEP of this element acquired in a certain polarization state. We can assume that the array is configured in an $\boldsymbol{S}_{1\times N}^{(0)}$ polarization state, and the VAEP of the nth array element is attained by using full-wave simulation. Then, when this

array is configured in another polarization state, $\boldsymbol{S}_{1\times N}^{(1)}$, the VAEP of the nth element can be approximated by the following formula:

$$\begin{aligned}\boldsymbol{E}_n\left(\theta,\phi;\boldsymbol{S}_{1\times N}^{(1)}\right)\approx{}& E_{n,\theta}\left(\theta,\phi+\varphi_n^{(0)}-\varphi_n^{(1)};\boldsymbol{S}_{1\times N}^{(0)}\right)\cdot\boldsymbol{e}_\theta\\&+E_{n,\phi}\left(\theta,\phi+\varphi_n^{(0)}-\varphi_n^{(1)};\boldsymbol{S}_{1\times N}^{(0)}\right)\cdot\boldsymbol{e}_\phi\end{aligned}\tag{10}$$

where $\varphi_n^{(0)}$ and $\varphi_n^{(1)}$ are the polarization azimuth angles of the nth element under the polarization states $\boldsymbol{S}_{1\times N}^{(0)}$ and $\boldsymbol{S}_{1\times N}^{(1)}$, respectively. $E_{n,\theta}\left(\theta,\phi+\varphi_n^{(0)}-\varphi_n^{(1)};\boldsymbol{S}_{1\times N}^{(0)}\right)$ and $E_{n,\phi}\left(\theta,\phi+\varphi_n^{(0)}-\varphi_n^{(1)};\boldsymbol{S}_{1\times N}^{(0)}\right)$ are respectively the $\boldsymbol{e}_\theta$- and $\boldsymbol{e}_\phi$-components of the nth element VAEP obtained under the $\boldsymbol{S}_{1\times N}^{(0)}$ polarization state configuration. In fact, Eq. (10) means that the VAEP of the nth element at the $\boldsymbol{S}_{1\times N}^{(1)}$ polarization state can be approximated by that element's VAEP at the $\boldsymbol{S}_{1\times N}^{(0)}$ polarization state after rotation with an angle of $(\varphi_n^{(0)}-\varphi_n^{(1)})$. On the xz-plane, the element pattern in the $\boldsymbol{S}_{1\times N}^{(1)}$ polarization state is approximated by the following:

$$\begin{aligned}\boldsymbol{E}_n\left(\theta,0^\circ;\boldsymbol{S}_{1\times N}^{(1)}\right)\approx{}& E_{n,\theta}\left(\theta,\varphi_n^{(0)}-\varphi_n^{(1)};\boldsymbol{S}_{1\times N}^{(0)}\right)\cdot\boldsymbol{e}_\theta+\\&E_{n,\phi}\left(\theta,\varphi_n^{(0)}-\varphi_n^{(1)};\boldsymbol{S}_{1\times N}^{(0)}\right)\cdot\boldsymbol{e}_\phi\end{aligned}\tag{11}$$

Thus, by substituting Eq. (11) into Eq. (4), the xz-plane pattern of the array working at the $\boldsymbol{S}_{1\times N}^{(1)}$ polarization state configuration can be approximately calculated by the following:

$$\begin{cases}\boldsymbol{F}_\theta\left(\theta,0^\circ;\boldsymbol{S}_{1\times N}^{(1)}\right)=\sum_{n=1}^{N}\boldsymbol{E}_{n,\theta}\left(\theta,0^\circ;\boldsymbol{S}_{1\times N}^{(1)}\right)\cdot\mathrm{e}^{\mathrm{j}\beta x_n\sin\theta}\approx\sum_{n=1}^{N}\boldsymbol{E}_{n,\theta}\left(\theta,\varphi_n^{(0)}-\varphi_n^{(1)};\boldsymbol{S}_{1\times N}^{(0)}\right)\cdot\mathrm{e}^{\mathrm{j}\beta x_n\sin\theta}\\\boldsymbol{F}_\phi\left(\theta,0^\circ;\boldsymbol{S}_{1\times N}^{(1)}\right)=\sum_{n=1}^{N}\boldsymbol{E}_{n,\phi}\left(\theta,0^\circ;\boldsymbol{S}_{1\times N}^{(1)}\right)\cdot\mathrm{e}^{\mathrm{j}\beta x_n\sin\theta}\approx\sum_{n=1}^{N}\boldsymbol{E}_{n,\phi}\left(\theta,\varphi_n^{(0)}-\varphi_n^{(1)};\boldsymbol{S}_{1\times N}^{(0)}\right)\cdot\mathrm{e}^{\mathrm{j}\beta x_n\sin\theta}\end{cases}\tag{12}$$

According to Eqs. (6) and (7), the CoP and XP patterns of the array under the $\boldsymbol{S}_{1\times N}^{(1)}$ polarization state configuration can be calculated by the following:

$$\begin{cases}\boldsymbol{F}_{\mathrm{co}}\left(\theta,0^\circ;\boldsymbol{S}_{1\times N}^{(1)}\right)=\boldsymbol{F}_\theta\left(\theta,0^\circ;\boldsymbol{S}_{1\times N}^{(1)}\right)\cdot\cos\left(\varphi_{\mathrm{d}}\right)+\boldsymbol{F}_\phi\left(\theta,0^\circ;\boldsymbol{S}_{1\times N}^{(1)}\right)\cdot\sin\left(\varphi_{\mathrm{d}}\right)\\\boldsymbol{F}_{\mathrm{X}}\left(\theta,0^\circ;\boldsymbol{S}_{1\times N}^{(1)}\right)=\boldsymbol{F}_\phi\left(\theta,0^\circ;\boldsymbol{S}_{1\times N}^{(1)}\right)\cdot\cos\left(\varphi_{\mathrm{d}}\right)-\boldsymbol{F}_\theta\left(\theta,0^\circ;\boldsymbol{S}_{1\times N}^{(1)}\right)\cdot\sin\left(\varphi_{\mathrm{d}}\right)\end{cases}\tag{13}$$

By implementing a one-time full-wave simulation of the MLPR array under the $\boldsymbol{S}_{1\times N}^{(0)}$ polarization configuration, we can obtain the precise VAEP of each element antenna under $\boldsymbol{S}_{1\times N}^{(0)}$. Then, all the VAEPs of the elements in other polarization configurations, such as $\boldsymbol{S}_{1\times N}^{(1)}$, can be approximately obtained by means of Eq. (10). These approximated VAEPs are used to evaluate the fitness function of Eq. (8) when different polarization configurations are used. However, this approximation process will introduce certain errors into the pattern optimization process, especially when the array polarization configuration is significantly changed from the one used to obtain the precise VAEPs. In order to address this issue, we propose a refined polarization state optimization strategy, which is described in the next subsection.

2.3. Refined polarization state optimization strategy

Since the applied VAEPs of the array elements are obtained by the approximation process in Eqs. (10) and (11), the CoP and XP patterns of the array described in Eq. (13) will have some approximation errors. Generally speaking, the accuracy of the patterns expressed in Eqs. (12) and (13) depends on the difference between the $\boldsymbol{S}_{1\times N}^{(0)}$ and $\boldsymbol{S}_{1\times N}^{(1)}$ polarization state configurations—the greater the difference, the worse the approximation accuracy. To reduce the discrepancy, we adopt the following polarization state optimization strategy.

At the initial step of this strategy, the polarization states of all N elements are set such that they minimize. This arrangement of polarization state only allows the array to achieve a few discrete polarizations. To realize arbitrary linearly polarized radiation of the array, we choose to optimize the element polarization states as follows. First, the approximated VAEPs of the elements are obtained by means of a full-wave simulation under the initial polarization state configuration ($\boldsymbol{S}_{1\times N}^{(0)}$) and the approximation method given in Eqs. (10) and (11). Next, through optimization algorithms such as GA and PSO, with the guidance of the fitness function in Eq. (8), the array can generate radiation in the desired polarization with constrained SLL and XPL, and its corresponding polarization state configuration, denoted as $\boldsymbol{S}_{1\times N}^{(1)}$, can be obtained. However, there is a discrepancy between such a synthesized pattern (using the approximated VAEPs) and the actual pattern (using actual VAEPs under the selected polarization state configuration). Then, a full-wave simulation is performed for the antenna array configured under $\boldsymbol{S}_{1\times N}^{(1)}$, and the VAEPs of each element can be updated. Thus, the polarization state configuration can be re-optimized with the optional element polarization states restricted to the vicinity of the $\boldsymbol{S}_{1\times N}^{(1)}$ polarization state configuration.

The optional polarization states for the nth element can be described as $s_n^{(2)}\in\left[s_n^{(1)}-m_2,s_n^{(1)}+m_2\right]$, where m_2 is a user-defined integer for the re-optimization (second optimization). The re-optimized polarization state configuration can be denoted as $\boldsymbol{S}_{1\times N}^{(2)}$. Such a refined polarization state configuration optimization should be executed multiple times until the radiation pattern generated by the array in the desired polarization meets the user's requirements. We can assume that the polarization state configuration of the MLPR antenna array is $\boldsymbol{S}_{1\times N}^{(0)}$ at the initial step (k = 0) and $\boldsymbol{S}_{1\times N}^{(k)}$ at the kth optimization step (k = 1, 2, …, K). Then, the CoP and XP patterns of the array at the kth optimization step are given by the following:

$$\begin{cases}\boldsymbol{F}_{\mathrm{co}}\left(\theta,0^\circ;\boldsymbol{S}_{1\times N}^{(k)}\right)\approx\sum_{n=1}^{N}\boldsymbol{E}_{n,\mathrm{co}}\left(\theta,\varphi_n^{(k-1)}-\varphi_n^{(k)};\boldsymbol{S}_{1\times N}^{(k-1)}\right)\cdot\mathrm{e}^{\mathrm{j}\beta x_n\sin\theta}\\\boldsymbol{F}_{\mathrm{X}}\left(\theta,0^\circ;\boldsymbol{S}_{1\times N}^{(k)}\right)\approx\sum_{n=1}^{N}\boldsymbol{E}_{n,\mathrm{X}}\left(\theta,\varphi_n^{(k-1)}-\varphi_n^{(k)};\boldsymbol{S}_{1\times N}^{(k-1)}\right)\cdot\mathrm{e}^{\mathrm{j}\beta x_n\sin\theta}\end{cases}\tag{14}$$

The overall process of the proposed refined polarization state optimization strategy for the MLPR antenna array is detailed in the Algorithm that follows. In this process, the discrete polarization state optimization problem can be regarded as a nonlinear integer programming problem. In general, stochastic optimization algorithms such as BGA [33], binary PSO (BPSO) [34], and binary differential evolution (BDE) [43] would be appropriate for solving this problem, since they are capable of finding a globally optimum solution. Here, we adopt a BGA as the optimization algorithm, and the detailed procedure is organized in the Subprocedure shown below. The BGA is a relatively effective and practical optimization method that has been utilized to solve a number of optimization problems in the field of array antennas [33]. Using the optimization mechanism of the BGA, the polarization state configuration will iteratively change toward a better solution under the guidance of the fitness function in Eq. (8).

In practical applications, we can store the optimized array polarization state configurations for all of the desired LPs given by the user; then, through a control device such as an FPGA, we can realize programming control of the array polarization. In that case, the array can generate any desired linearly polarized wave radiation with constrained SLL and XPL by controlling the polarization state configuration using an FPGA.

Algorithm. The proposed refined polarization state optimization algorithm for the MLPR antenna array.

1: Initialize the number of elements N and the number of polarization states M of the element, and set the desired LP ($\boldsymbol{P}_{\mathrm{d}}$) and the desired maximum SLL (Γ_{SLL}) and XPL (Γ_{XPL});
2: Set $k = 0$ and initialize the MLPR antenna array polarization state configuration ($\boldsymbol{S}_{1\times N}^{(0)}$) by choosing one polarization state for each element in order to have a minimize value of $|\varphi_n - \varphi_{\mathrm{d}}|$ for $n = 1, 2, \ldots, N$;
3: Set $k = k + 1$, and set the optional polarization state range $s_n^k \in \left[s_n^{(k-1)} - m_k, s_n^{(k-1)} + m_k\right]$ for $n = 1, 2, \ldots, N$;
4: Obtain the approximated VAEPs of each element for all the optional polarization states by using the approximation method in Eqs. (10) and (11);
5: Perform the BGA-based polarization states optimization in the subprocedure below with the guidance of the fitness function (Eq. (8)) to find the best polarization state configuration $\boldsymbol{S}_{1\times N}^{(k)}$ of the MLPR antenna array so as to generate a pattern with the desired polarization $\boldsymbol{P}_{\mathrm{d}}$ and constrained SLL and XPL;
6: Full-wave simulate the actual antenna array whose elements are working at the optimized polarization state configuration $\boldsymbol{S}_{1\times N}^{(k)}$ to obtain the actual array pattern, and update the VAEP of each element at the current polarization state configuration;
7: Check whether the difference between the synthesized and actual array patterns meets the specified tolerance. If yes, then exit the whole procedure; otherwise, repeat Steps 3 to 7.

Subprocedure. The BGA-based polarization states selection procedure.

1: Initialize the population size N_{p}, individual length L, mutation probability P_{m}, crossover probability P_{c}, and maximum iteration number I_{m}. Note that L usually satisfies $2^{L-1} < M \leq 2^L$, where M is the number of polarization states for the adopted reconfigurable antenna element. Hence, an individual has a binary code of $(N \cdot L)$ bits, representing the polarization state configuration of the N-element MLPR antenna array;
2: Randomly generate S individuals to form an initial population and calculate the fitness score of each individual using Eq. (8). Set the iteration number $t = 0$;
3: Sort the individuals by their fitness score in ascending order. Random copy operations are performed on individuals according to their copy probability. The copy probability is calculated as follows: $g_i = \frac{e(1-e)^{i-1}}{\sum_i^{N_{\mathrm{p}}} e(1-e)^{i-1}}$ where i is the rank order of the individual, $e \in (0, 1)$ is the copy coefficient given by the user, and g_i represents the copy probability of the individual whose fitness score is sorted at the ith place. The higher the fitness score, the greater the probability of survival;
4: According to the mutation probability P_{m}, some individuals are randomly selected for mutation. The mutation position is chosen randomly and independently for each selected individual. The selected bit will mutate to "1" if it was originally "0." Otherwise, it mutates to "0" from "1;"
5: According to the crossover probability P_{c}, an even number of individuals are randomly selected from the population to cross over. The selected individuals are randomly paired, and each pair of chromosomes cross over at a random position;
6: Calculate the fitness score of each individual by means of Eq. (8), and record the current optimal individual and its fitness score;
7: Set $t = t + 1$ and repeat Steps 3 to 7 until $t > I_{\mathrm{m}}$ or until the best fit solution remains unchanged for multiple iterations.

3. The antenna array design

In this section, an MLPR patch antenna with eight LP states is designed and used to construct a 16-element polarization reprogrammable antenna array. Then, the polarization state configuration of the antenna array is optimized by the proposed strategy to achieve array patterns with several different polarizations so as to validate the concept of the polarization programmable antenna array.

3.1. The MLPR element antenna design and its simulated performances

An eight-LP reconfigurable antenna is developed as the array element. The element is based on a ring slot patch structure that can realize 360° polarization scanning with a 22.5° interval [23]. As shown in Fig. 3(a), the antenna element consists of double layers of substrates with a 3.7 mm air gap between them. A fiberglass epoxy copper clad laminate (FR-4) substrate with a dielectric constant (ε_r) of 4.4 and a loss tangent ($\tan\delta$) of 0.009 is used for both substrates 1 and 2. The thicknesses of substrates 1 and 2 are 0.6 and 0.3 mm, respectively. The reconfigurable radiator of the antenna is printed on the top surface of substrate 1, as shown in Fig. 3(b). The radiator is a circular patch that is separated into two parts by a ring slot. The part of the radiator outside the ring slot is evenly divided into 16 pieces by 16 gaps to realize the polarization reconfigurability. PIN diodes lie between these 16 pieces and the inside circular patch, and serve as the polarization reconfigurability switches. On the outer edge of the radiator patch, 16 pads are evenly printed for direct current (DC) biasing. Inductors are bridged between these DC pads and the radiator patch; they can block RF signals while maintaining the DC conduction. The ground plane of the antenna is printed on the bottom surface of substrate 1. There is a circular patch on the top surface of substrate 2, as shown in Fig. 3(c). This circular patch acts as a parasitic patch to improve the antenna performance. The element antenna is fed by a 50 Ω coaxial cable, as shown in Fig. 3(a). The inner and outer conductors of the coaxial cable are separately connected to the central circular patch on the top of substrate 1 and to the ground plane on the bottom of substrate 1. Metallic posts passing vertically through substrate 1 are used as the DC bias lines, which are connected to the pads on the top surface of substrate 1. The detailed dimensions of the developed antenna are provided in the caption of Fig. 3.

The PIN diode adopted here is Bar50-02 V with 0603 packaging, produced by Infineon. In the On state, this diode is equivalent to a 3 Ω resistor in series with a 0.6 nH inductor, while in the Off state, it is equivalent to a 5000 Ω resistor in parallel with a 0.1 pF capacitor and in series with a 0.6 nH inductor (for details of its performance, interested readers can refer to Ref. [44]). The inductor used is VHF100505HQ4N7ST with 0402 packaging and an inductance value of 4.7 nH, produced by FengHua Advanced Technology Company. It can effectively block the 4.5–5.5 GHz RF signal while keeping the DC continuous [45]. When the developed antenna is working, eight adjacent PIN diodes are turned on at

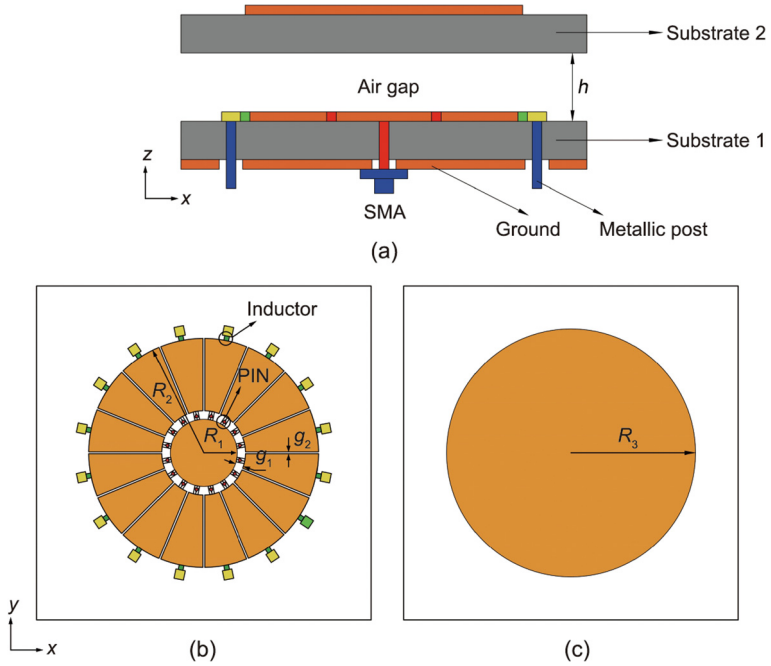

Fig. 3. Geometry of the proposed eight-LP reconfigurable circular patch antenna. (a) Sectional drawing along the *x*-axis; (b) top view of substrate 1; (c) top view of substrate 2. The antenna dimensions are: the radius of inside circular patch R_1 = 3.6, the radius of the radiator patch R_2 = 8.65, the radius of the parasitic patch R_3 = 10.5, the width of the ring slot g_1 = 0.5, the width of the dividing gaps g_2 = 0.2, and the height of the air gap h = 3.7 (unit: mm). SMA: sub-miniature version A.

the same time. When a PIN diode is on, its cathode is connected to the negative pole of a DC source through the center circular patch and the inner conductor of the coaxial cable, while the anode of the diode is biased to the positive pole of the DC source through the metallic post. In Fig. 4, the red part indicates conduction, while the blue part indicates blockage. As a result, the antenna is working at a 0° polarization state. By rotating the configuration of the On–Off states of these PIN diodes in the circular direction, the antenna can generate eight different LPs with a 22.5° interval.

The simulation software High Frequency Structure Simulator (HFSS) is used to simulate the developed antenna element. Due to the rotation symmetry of this antenna, the performances of the antenna at different polarization states are almost the same. Thus, for simplicity, here we only give the performance of the antenna working at a polarization state of 0°. As shown in Fig. 5(a), the simulated bandwidth is 12.2% covering 4.63–5.23 GHz (when the return loss ($|S_{11}|$) of the antenna is less than −10 dB). The radiation pattern of the antenna at 5 GHz is shown in Fig. 5(b). The simulated gain at 5 GHz is 7.2 dBi with XPL ≤ −25 dB. To check the effect of the PIN diodes on the antenna gain and efficiency, we simulate the antenna with two different PIN diode models: Model A, which adopts the equivalent circuit model of the PIN diode, as described above, and Model B, which ideally regards the On and Off states of the diode as the "connection" and "disconnection" of a perfect electric conductor (PEC) stripline. The simulated gain and radiation efficiency of the antenna using these two models are shown in Fig. 6. As shown in the figure, compared with the ideal PIN Model B, the antenna using PIN Model A suffers from a gain degradation of 0.5–1 dB in the 4.63–5.23 GHz band, as well as from an efficiency reduction of 5%–10%. This loss in gain and efficiency can mostly be attributed to the insertion losses of these PIN diodes. As a result, within the working band, the realized gain of the antenna using the more realistic PIN Model A ranges from 5.83 to 7.48 dBi, and the radiation efficiency ranges from 59.69% to 80.15%, as shown in Fig. 6.

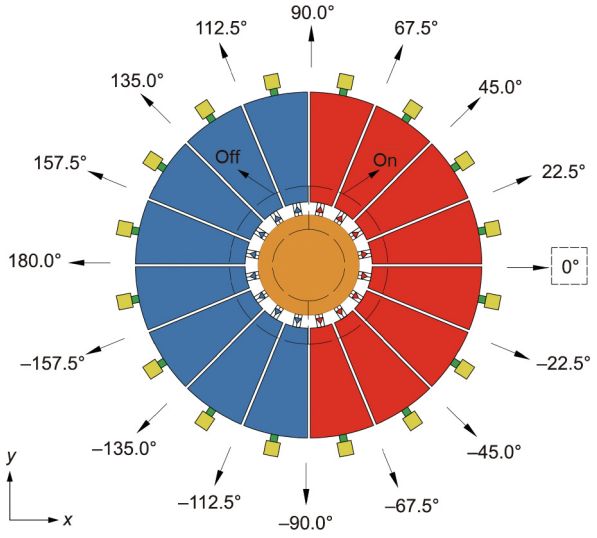

Fig. 4. The realizable polarization states of the developed MLPR antenna. Red diodes are on, while blue diodes are off. Under this configuration, the antenna achieves a polarization state of 0°.

3.2. Verification and analysis of the element pattern approximation method

Using the developed MLPR antenna element described above, we constructed a 16-element uniform linear MLPR antenna array with an element spacing of 30 mm (half wavelength at 5 GHz). The port isolation between different elements is generally taken as one of the important performance indexes. For the proposed MLPR antenna array, the port isolation would be affected by the

polarization states of different elements. To study the effect of varying polarization states on the port isolation, we check the parameter $|S_{78}|$ of the array (port isolation between the seventh and eighth elements) by changing the polarization state of the eighth element from 0° to 90° with an interval of 22.5°, while all the other elements are kept at a state of 0°. The full-wave simulated $|S_{78}|$ curves at different polarization states of the eighth element are shown in Fig. 7. It can be seen that, as the polarization direction angle difference between the seventh and eighth elements increases, the maximum value of $|S_{78}|$ within the frequency band (4.5–5.5 GHz) decreases gradually from −22 to −56 dB. This is reasonable, since the port isolation between two elements in CoP states is usually much higher than that of two elements in orthogonal-polarization states.

On the other hand, the element patterns in the array environment generally vary with different elements, due to mutual coupling. In addition, for the developed MLPR antenna array, the element pattern shapes could be affected by the element polarization state distribution. Thus, there may exist some approximation errors when we adopt Eq. (10) to obtain the pattern for an array element at a new polarization state by mathematically rotating the pattern of this element obtained at one polarization state. To analyze the performance of such an approximation in Eq. (10), we switch the polarization state of the eighth element from the 0° state to the [22.5°, 45.0°, 67.5°, 90.0°] states, and then compare the VAEPs of this element, which are obtained by full-wave simulating the whole array, with the corresponding results obtained by using the approximation method of Eq. (10). Here, we denote the VAEPs of the eighth element in the [0°, 22.5°, 45.0°, 67.5°, 90.0°] states as $\boldsymbol{E}_8(\theta,\phi,\boldsymbol{S}^{(0)}_{1\times N})$, $\boldsymbol{E}_8(\theta,\phi,\boldsymbol{S}^{(1)}_{1\times N})$, $\boldsymbol{E}_8(\theta,\phi,\boldsymbol{S}^{(2)}_{1\times N})$, $\boldsymbol{E}_8(\theta,\phi,\boldsymbol{S}^{(3)}_{1\times N})$, and $\boldsymbol{E}_8(\theta,\phi,\boldsymbol{S}^{(4)}_{1\times N})$, respectively. For the case when the observation plane is the *xz*-plane ($\phi = 0°$), the approximated and actual VAEPs of the eighth element are shown in Fig. 8 for comparison. As shown in Fig. 8(a), the approximated VAEP of the eighth element at the state of 22.5° that is obtained by mathematically rotating the VAEP of the eighth element at the 0° state agrees well with the actual VAEP of the eighth element at the state of 22.5°. The error between the approximated and actual VAEPs of the eighth element at the state of 45° is acceptable, as shown in Fig. 8(b). However, as shown in Fig. 8(c), the difference between the approximated VAEP at the state of 67.5°, as obtained from the mathematical rotation of the VAEP at the 0° state, and the actual VAEP at the state of 67.5° is fairly large. Moreover, as shown in Fig. 8(d), a significant difference exists between the approximated VAEP at the state of 90° and the actual one. This is because the element mutual coupling will change with the switching of the polarization states. Generally speaking, the greater the angle of mathematical rotation is, the greater the change in the mutual coupling of the array elements will be, resulting in greater approximation errors. Hence, in order to obtain a more reliable pattern of the MLPR array by optimizing the element polarization states, we use the refined strategy proposed in Section 2.3 to reduce the error caused by the approximation.

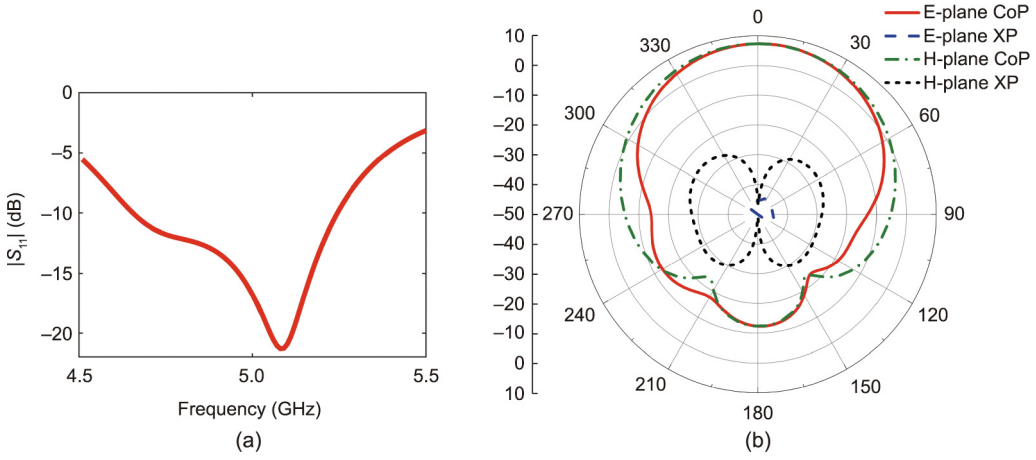

Fig. 5. The simulated performances of the developed MLPR antenna at a polarization state of 0°: (a) $|S_{11}|$ and (b) the E- and H-plane patterns at 5 GHz. E-plane: the plane composed of the maximum radiation direction of the antenna and the direction of the electric field; H-plane: the plane composed of the maximum radiation direction of the antenna and the direction of the magnetic field.

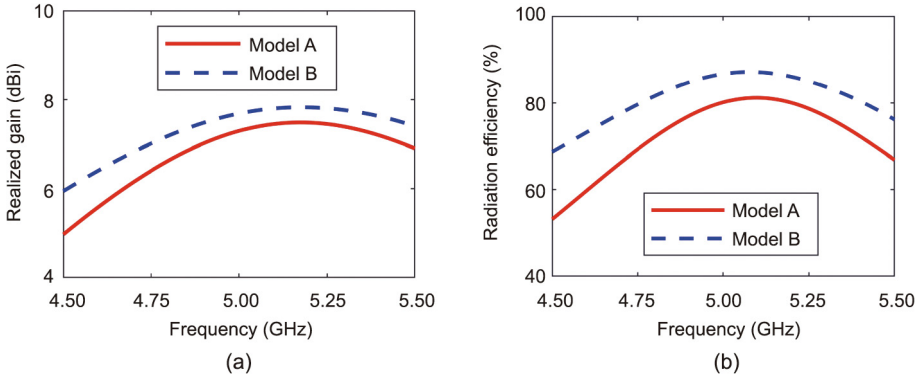

Fig. 6. (a) The realized gain curves (simulated) and (b) radiation efficiencies (simulated) of the MLPR antenna element using two different PIN diode models. Model A: equivalent circuit model; Model B: ideal model.

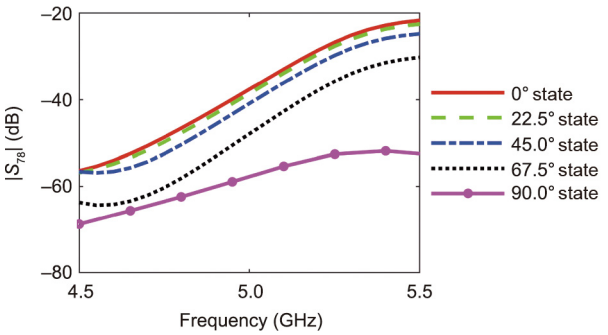

Fig. 7. The simulated $|S_{78}|$ of the antenna array when the polarization state of the eighth element switches from the 0° state to the 90° state. The polarization states of other elements are kept at the 0° state.

3.3. Validation of the reprogrammable antenna array concept

Now, to validate the concept of the polarization programmable antenna array, the proposed refined strategy is adopted in order to optimize the polarization state configuration of the 16-element array for several different desired polarizations. It should be noted that, although the developed polarization reconfigurable element antenna can only achieve eight LP states, its VAEPs are actually different among the 16 working states. For example, one element antenna is regarded as operating at the same polarization when it is working at the polarization states of 0° and 180°, but the VAEPs of the antenna in these two states are different. This is because both the radiated vectorial electromagnetic field and the mutual coupling between this element and its neighboring elements are different in these two states. Thus, in the polarization state optimization, the element antenna is regarded as having 16 different polarization states. The polarization azimuth angles of these 16 polarization states are {0°, 22.5°, 45.0°, ..., 315.0°, 337.5°}, with an interval of $\Delta\phi = 22.5^{\circ}$.

As the first validation example, the polarization states of each MLPR antenna in the array are optimized using the proposed strategy to achieve a vectorial radiation pattern with a desired polarization $\boldsymbol{P}_{\mathrm{d}}$ of (90°, 30°). This desired polarization state cannot be realized by the adopted element antennas themselves; however, we can make the array radiate in the desired polarization with a constrained SLL and XPL by optimizing its polarization state configuration. The desired SLL (Γ_{SLL}) and the desired XPL (Γ_{XPL}) are set as −18.0 dB. In the subprocedure of the BGA-based polarization states optimization, we set N_{p} = 200 for the population size, I_{m} = 400 for the maximum number of iterations, $P_{\mathrm{c}} = P_{\mathrm{m}} = 0.6$ for the individual-crossover and mutation possibility, and $W_1 = W_2 = 0.5$ for the weighting factor in the fitness function (Eq. (8)). At the initial step (k = 0), all elements are adjusted to work at the polarization state of 22.5°, which is the closest to the desired $\boldsymbol{P}_{\mathrm{d}} = (90^{\circ}, 30^{\circ})$. It is well-known that such a uniform polarization state configuration usually generates a pattern with an SLL of approximately −13.5 dB, as shown in Fig. 9(a). Then, this array can be full-wave simulated by using HFSS, and all the VAEPs of the elements under such a polarization state configuration can be obtained. By applying the approximation method in Eqs. (10) and (11), we can obtain the approximated VAEPs. Thus, the polarization state configuration of the array can be optimized by performing the BGA optimization (k = 1).

Here, in order to release more degrees of freedom to improve the pattern performance of the array, we do not restrict the polarization state configuration of the array to be symmetrical. The CoP and XP patterns of the array working in the first optimized polarization state configuration are shown in Fig. 9(b). As shown in the figure, the SLL is −17.88 dB and the XPL is −17.92 dB, both of which are very close to the desired values. However, due to the change of the mutual coupling between elements, the actual array pattern at the first optimized polarization state configuration obtained by full-wave simulation only has an SLL of −14.96 dB and an XPL of −16.80 dB. To reduce the difference between the optimized and actual array patterns, several refining steps are

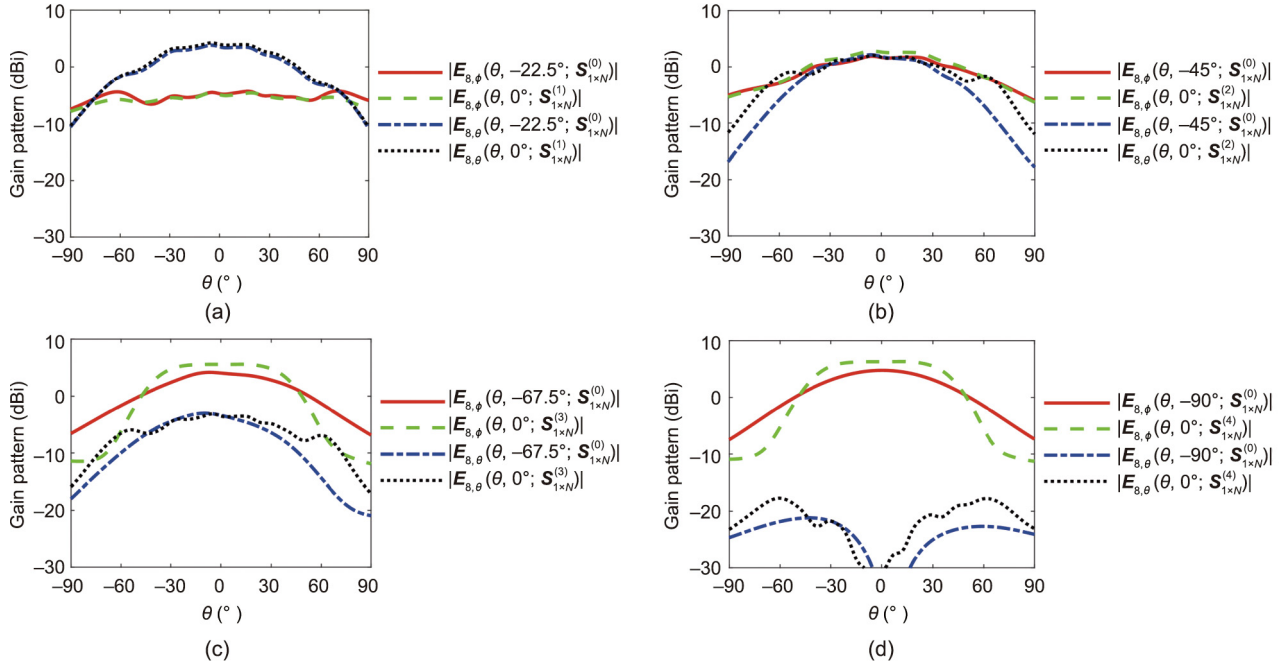

Fig. 8. Comparison of the approximated VAEPs obtained by mathematically rotating the VAEP of the eighth element at the 0° state and the actual VAEPs obtained by full-wave simulating the eighth element at different polarization states. (a) 22.5° state; (b) 45° state; (c) 67.5° state; (d) 90° state. The observation plane is the *xz*-plane.

adopted to re-optimize the element polarization states, as described in the Algorithm. The range of the allowable optional polarization states is assigned as monotonically diminishing values with an increasing number of refining steps. Here, we set $m_2 = 2$ and $m_3 = 1$ at the second and third optimization step (at the first optimization step, all the polarization states can be selected for each element). That is, the optional polarization state range for the nth element is set as $s_n^{(2)} \in \left[s_n^{(1)} - 2, s_n^{(1)} + 2\right]$ and $s_n^{(3)} \in \left[s_n^{(2)} - 1, s_n^{(2)} + 1\right]$. Therefore, at the second optimization step ($k = 2$), there are five optional polarization states for the nth element: namely, the polarization state obtained at the first optimization step and its four nearby polarization states. At the third optimization step ($k = 3$), the available polarization states for the nth element include the polarization state obtained at the second optimization step and its two nearby polarization states. Figs. 9(c) and (d) show the optimized and actual patterns of the array working at the polarization state configurations obtained at the second and third optimization steps (two refining steps), respectively. As shown in the figure, at the third optimization step, the actual array pattern is very similar to the optimized one. The obtained SLL and XPL of the actual array pattern are reduced to −17.61 and −17.26 dB, respectively. At the third optimization step, the optimized polarization states of the array have only a few changes in comparison with those obtained at the second optimization step. The polarization state configurations obtained at the initial step and the three optimization steps are listed in Table 1, and the corresponding SLLs and XPLs obtained at each step are given in Table 2 for comparison. It can be seen that, when $k = 1$, the difference between the optimized SLL and the actual SLL is 2.92 dB. When $k = 3$, this difference decreases to 0.09 dB. The SLL of the actual pattern is reduced from −14.96 to −17.61 dB. In general, as more refining steps are applied, the SLL and XPL of the actual array pattern are gradually reduced and increasingly approach those of the synthesized pattern. In this example, a total of three BGA-based optimizations of the 16-element polarization states and four HFSS full-wave simulations of the 16-element MLPR antenna array are performed. On average, each BGA optimization takes 3.88 min, and a full-wave simulation takes 83.64 min (on a Dell Workstation with an Intel Xeon E5-2697 central processing unit (CPU) at 2.30 GHz and 512 GB RAM). Thus, the time cost of the whole process is about 346.20 min, of which the full-wave simulation takes about 334.56 min. Although it is relatively time-consuming to obtain the VAEPs by means of full-wave simulation, the proposed method can effectively enable the MLPR antenna array to generate a pattern with a desired LP while taking mutual coupling into consideration.

Similarly, appropriate polarization state configurations are obtained with the proposed refined strategy when the desired

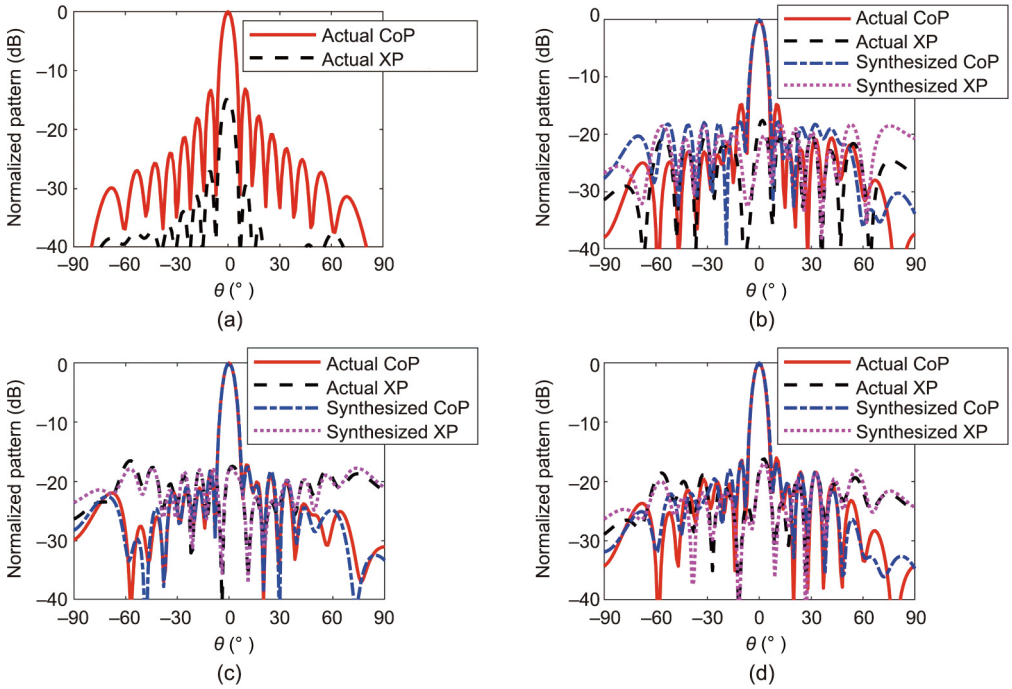

Fig. 9. The synthesized patterns and corresponding actual array patterns obtained by full-wave simulation at the initial step and three optimization steps of the MLPR antenna array, when the desired polarization is (90°, 30°). (a) The actual pattern under the initial polarization state configuration; (b)–(d) the results at the (b) first, (c) second, and (d) third optimization step.

Table 1
The polarization state configurations obtained by the proposed method at the initial step and three optimization steps when the desired polarization is (90°, 30°).

k	16-element polarization state (°)															
	1	2	3	4	5	6	7	8	9	10	11	12	13	14	15	16
0	22.5	22.5	22.5	22.5	22.5	22.5	22.5	22.5	22.5	22.5	22.5	22.5	22.5	22.5	22.5	22.5
1	22.5	−45.0	67.5	22.5	45.0	22.5	22.5	22.5	22.5	22.5	45.0	22.5	45.0	0	67.5	22.5
2	45.0	−22.5	22.5	22.5	45.0	22.5	22.5	22.5	22.5	22.5	45.0	22.5	67.5	−45.0	90.0	22.5
3	45.0	−22.5	22.5	22.5	45.0	22.5	22.5	22.5	45.0	22.5	45.0	22.5	90.0	−45.0	90.0	0

polarization is (90°, 0°), (90°, 45°), (90°, 60°), and (90°, 90°), respectively. The desired polarization of (90°, 60°) cannot be achieved by the adopted antenna element itself. Like the above example with a desired polarization of (90°, 30°), we can use the proposed method to enable the array to radiate in the desired polarization with a constrained SLL and XPL. When the desired polarizations are (90°, 0°), (90°, 45°), and (90°, 90°), the array can generate radiation patterns in the desired polarization by switching all the elements to work at the corresponding polarization states. However, this results in a pattern with an SLL of about −13.5 dB. Due to mutual coupling between the array elements, the SLL may even deteriorate. By optimizing the element polarization states, we can reduce the SLL of this array. The synthesized and actual array patterns with the four polarization directions obtained by the proposed polarization state optimization strategy are shown in Figs. 10(a)–(d), respectively. The obtained polarization state configurations are listed in Table 3, and the corresponding SLLs and XPLs are listed in Table 4. As can be seen, the obtained SLLs and XPLs of the actual array pattern for the four different LPs are all better than −16.5 dB. Although only five LP directions are considered in total, it can be reasonably concluded that the MLPR antenna array can achieve patterns with any desired LPs, and with both reduced SLLs and constrained XPLs, simply by adopting the optimized polarization states of the antenna elements through the proposed strategy. In addition, since no excitation amplitude or phase optimization is involved for the polarization programmable antenna array, the beamforming network of this array is greatly simplified.

Table 2
The maximum SLL and XPL of the synthesized and actual array pattern at the initial step and three optimization steps for the MLPR antenna array when the desired polarization is (90°, 30°).

k	Synthesized results (dB)		Simulated results (dB)	
	SLL	XPL	SLL	XPL
0	–	–	−13.39	−14.73
1	−17.88	−17.92	−14.96	−16.80
2	−17.42	−17.40	−16.57	−16.66
3	−17.70	−17.31	−17.61	−17.26

4. Experimental results

The antenna array described above was fabricated and measured to further validate the proposed concept of the polarization programmable array and the optimization strategy. Figs. 11(a) and (b) show photographs of the top view and bottom view of the prototype array. In order to facilitate the On and Off control of a large number

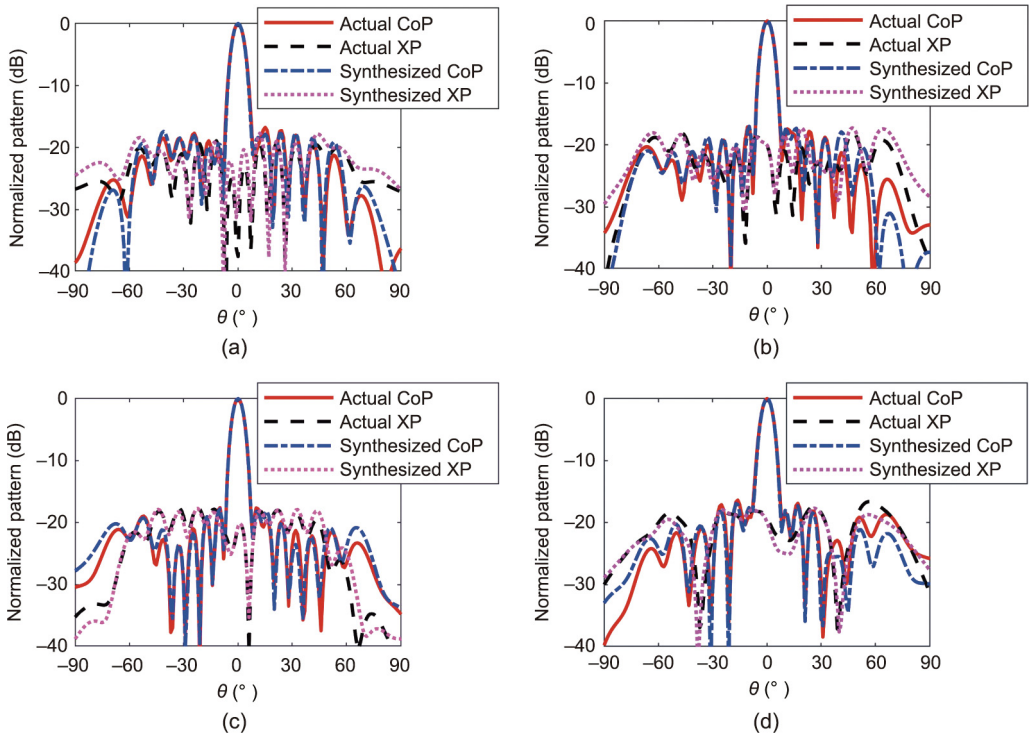

Fig. 10. The synthesized CoP and XP patterns and corresponding actual array patterns obtained by the full-wave simulation of the MLPR antenna array. (a)–(d) The obtained patterns for the desired polarization of (a) (90°, 0°), (b) (90°, 45°), (c) (90°, 60°), and (d) (90°, 90°).

Table 3
The polarization state configurations of the MLPR array obtained by the proposed refined optimization strategy when the desired polarizations are (90°, 0°), (90°, 45°), (90°, 60°), and (90°, 90°).

P_d	16-element polarization state (°)															
	1	2	3	4	5	6	7	8	9	10	11	12	13	14	15	16
(90°, 0°)	0	−45.0	0	0	22.5	0	0	0	0	0	0	−22.5	45.0	−90.0	90.0	0
(90°, 45°)	45.0	67.5	45.0	67.5	45.0	45.0	45.0	45.0	45.0	45.0	45	22.5	67.5	−22.5	135.0	45.0
(90°, 60°)	67.5	45.0	67.5	67.5	67.5	67.5	67.5	67.5	67.5	67.5	45	67.5	0	45.0	157.5	67.5
(90°, 90°)	135.0	0	90.0	−22.5	112.5	90.0	67.5	90.0	90.0	90.0	90	90.0	90.0	90.0	90.0	0

Table 4
The SLL and XPL of the pattern of the MLPR array obtained by the proposed refined optimization strategy when the desired polarizations are (90°, 0°), (90°, 45°), (90°, 60°), and (90°, 90°).

P_d	Synthesized results (dB)		Simulated results (dB)	
	SLL	XPL	SLL	XPL
(90°, 0°)	−17.53	−17.39	−17.30	−17.66
(90°, 45°)	−17.07	−17.90	−17.00	−17.81
(90°, 60°)	−17.59	−17.57	−17.53	−17.46
(90°, 90°)	−17.04	−17.52	−16.53	−16.76

of PIN diodes and actualize the programmable array polarizations, an FPGA DC control circuit was designed and processed, as shown in Figs. 11(c) and (d). The polarization states of the element antenna are encoded in four-bit binary code, as {0000, 0001, . . ., 1111}, corresponding to {0°, 22.5°, . . ., 337.5°} states. In this way, the polarization state configuration of the 16-elememt array is encoded into 64-bit binary codes. The obtained polarization state configurations are stored in Table 5, corresponding to the five desired LPs of (90°, 0°), (90°, 30°), (90°, 45°), (90°, 60°), and (90°, 90°). When measuring the MLPR antenna array for different desired polarizations, we have the FPGA supply power to the DC bias network through the corresponding binary code; then, the array polarization state can be switched. The simulated and measured gain patterns at 5 GHz of the array under the five optimized polarization state configurations are shown in Fig. 12. It should be noted that, unlike the simulated patterns in Figs. 9 and 10 (which are fed by 16 individual coaxial ports in the HFSS model), the actual patterns depicted in Fig. 12 are obtained by simulating the whole antenna array, fed by equal power dividers. Hence, there is a small difference between the simulated patterns in Figs. 9 and 10 and the simulated patterns in Fig. 12. As shown in Fig. 12, for these five desired polarizations, the array can generate radiation patterns with relatively low SLLs when the array elements are working on the optimized polarization states. The simulated and measured SLLs and XPLs, as well as the realized gains of the MLPR antenna array at 5 GHz, are given in Table 6. It can be seen that, for the five cases with different desired LPs, the measured SLLs and XPLs are all better than −16.0 dB and the measured gains are above 16.7 dBi; however, they are about 0.5–1.0 dB lower than the simulated ones, which is caused by a non-ideal measurement environment and fabrication errors such as the effect of welding. Despite the imperfections, the measured CoP and XP patterns are generally in good agreement with the simulated ones.

Fig. 13 shows the simulated and measured reflection coefficients, gain curves, and radiation efficiencies of the array working in the five optimized polarization state configurations. Since the nonuniformly distributed element polarization state may affect the gain and bandwidth of the array, Fig. 13 also shows the performances of the array when the element polarization states are consistent with the 0° state, the 45° state, and the 90° state, respectively, as comparisons. These polarization state configurations are denoted in the figure as the Uniform (90°, 0°) state, Uniform (90°, 45°) state, and Uniform (90°, 90°) state. As shown in Fig. 13(a), the reflection coefficient of the MLPR antenna array slightly differs under different polarization state configurations. The overlapped bandwidth of the array is about 8.6%, covering 4.77–5.20 GHz. It should be noted that the bandwidth performance of this array is mainly limited by its elements, since its feed network is a parallel network with a relatively large bandwidth. As shown in Fig. 13(b), compared with the simulated gains, the measured gains are reduced by about 0.5–1.0 dB. Within the working band, the measured gains of the array under the Uniform (90°, 0°) state, Uniform (90°, 45°) state, and Uniform (90°, 90°) state range from 15.22 to 17.92 dBi, and the gain range of the array under the five optimized polarization state configurations is 14.84–17.53 dBi. Compared with the gains of the array under the Uniform states, the gains of the array with the optimized polarization state configurations are reduced by around 0.4–0.7 dB. This is because cancellation occurs among elements with different polarization states, which may have a negative effect on the CoP gain.

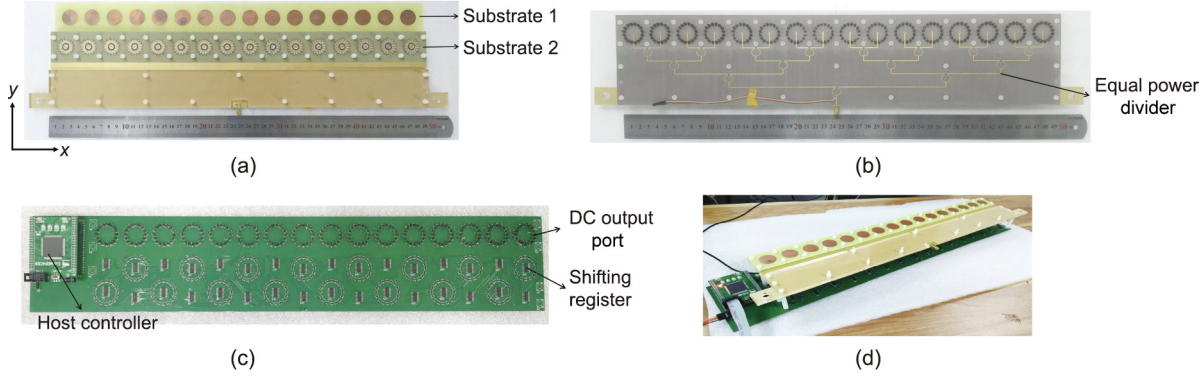

Fig. 11. Photographs of the 16-element MLPR antenna array prototype and its control circuit. (a) Top view of the array (incomplete assembly); (b) bottom view of the array; (c) FPGA control board of the array; (d) assembled polarization programmable array.

Table 5
The binary codes of the obtained polarization state configurations when the desired polarizations are (90°, 0°), (90°, 30°), (90°, 45°), (90°, 60°), and (90°, 90°).

P_d	Polarization state configuration codes															
	1	2	3	4	5	6	7	8	9	10	11	12	13	14	15	16
(90°, 0°)	0000	1101	0000	0000	0001	0000	0000	0000	0000	0000	0000	1110	0010	1010	0101	0000
(90°, 30°)	0010	1110	0001	0001	0010	0001	0001	0001	0010	0001	0010	0001	0101	1101	0101	0001
(90°, 45°)	0010	0011	0010	0011	0010	0010	0010	0010	0010	0010	0010	0001	0011	1110	0111	0010
(90°, 60°)	0011	0010	0011	0011	0011	0011	0011	0011	0011	0011	0010	0011	0000	0010	0111	0011
(90°, 90°)	0111	0000	0101	1110	0110	0101	0011	0101	0101	0101	0101	0101	0101	0101	0101	0000

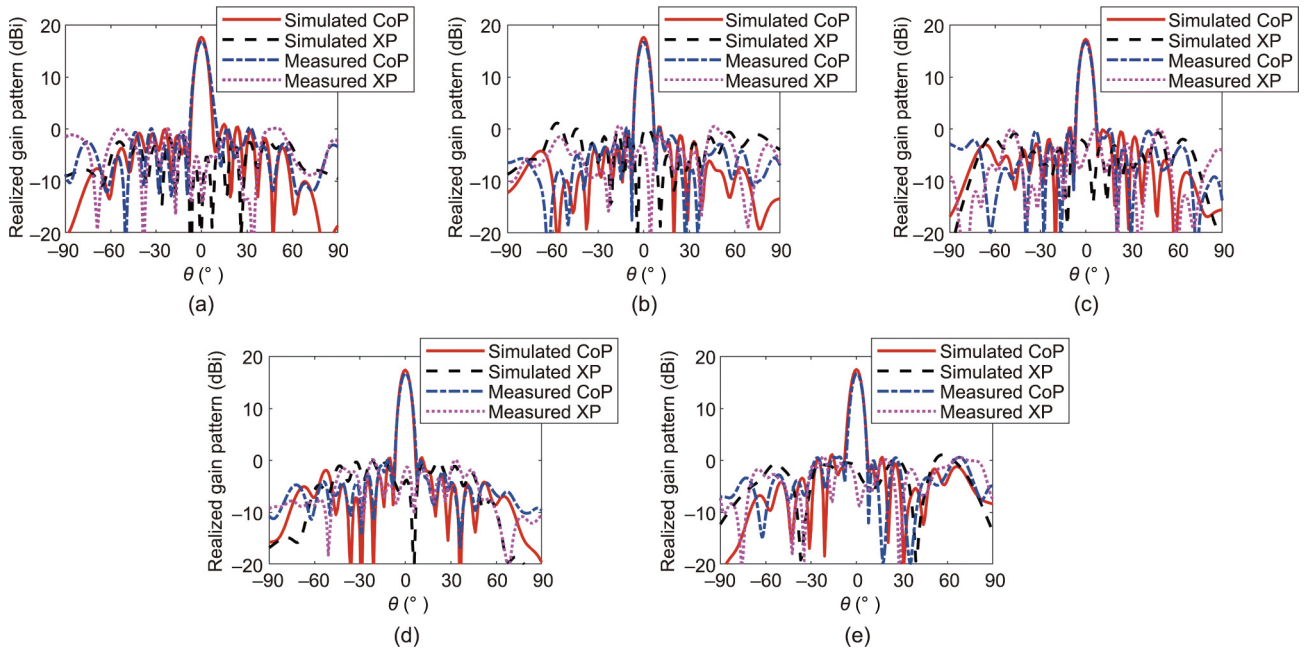

Fig. 12. The measured and simulated patterns of the MLPR antenna array when the desired polarizations are (a) (90°, 0°); (b) (90°, 30°); (c) (90°, 45°); (d) (90°, 60°); and (e) (90°, 90°).

Table 6
The simulated and measured SLL, XPL, and gain of the MLPR antenna array at 5 GHz when the desired polarizations are (90°, 0°), (90°, 30°), (90°, 45°), (90°, 60°), and (90°, 90°).

P_d	Simulated results			Measured results		
	SLL (dB)	XPL (dB)	Realized gain (dBi)	SLL (dB)	XPL (dB)	Realized gain (dBi)
(90°, 0°)	−16.80	−18.56	17.683	−16.58	−16.72	16.854
(90°, 30°)	−17.36	−16.59	17.671	−16.55	−16.15	16.737
(90°, 45°)	−17.07	−18.02	17.299	−16.78	−16.70	16.709
(90°, 60°)	−16.91	−17.34	17.425	−16.81	−16.72	16.782
(90°, 90°)	−16.43	−16.46	17.522	−16.09	−16.03	16.743

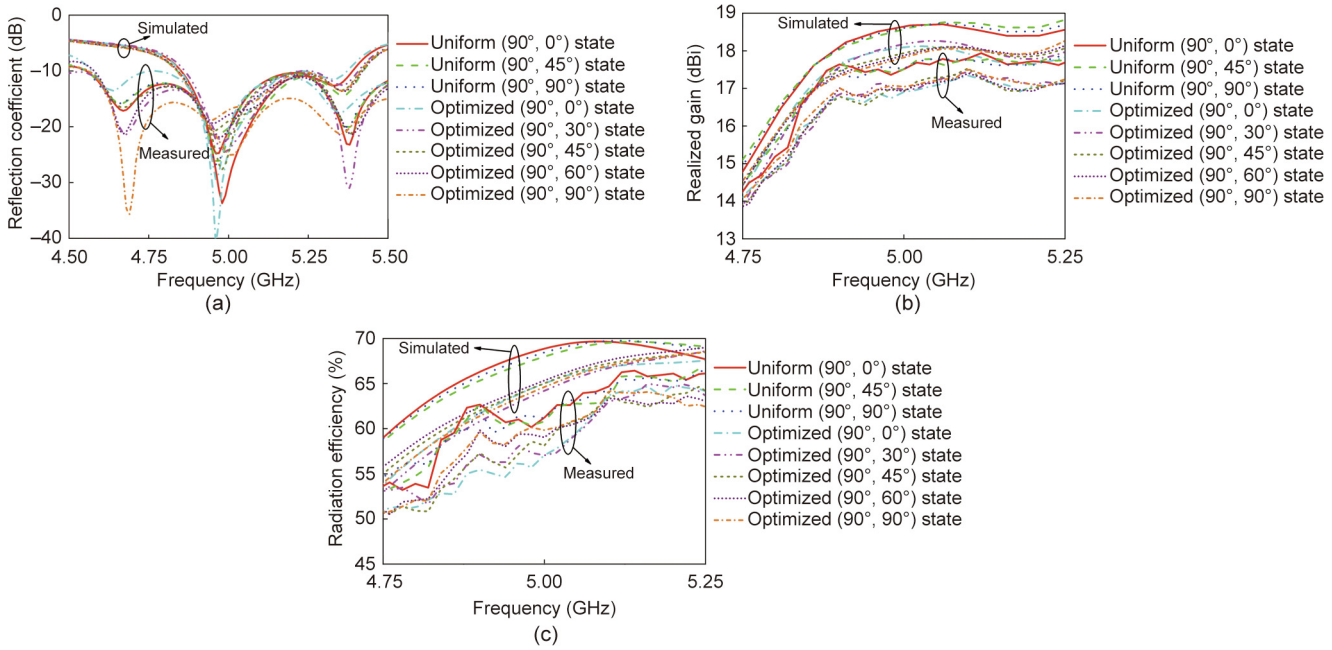

Fig. 13. The measured and simulated performances of the MLPR antenna array under the five optimized polarization state configurations and the Uniform (90°, 0°) state, Uniform (90°, 45°) state, and Uniform (90°, 90°) state. (a) Reflection coefficients; (b) realized gains; (c) radiation efficiencies.

Nevertheless, the MLPR array will produce an SLL of −13.5 dB under uniform polarization state configurations. The proposed approach provides an optional polarization state configuration for reducing the SLL of the MLPR antenna array. In practical applications, if a small quantity of gain loss is acceptable, then the optimized array polarization state configuration can be used to obtain a pattern with reduced SLL. If an SLL of −13.5 dB is acceptable, then the Uniform state can be selected to obtain a higher gain. As shown in Fig. 13(c), within the working band, the measured radiation efficiency of the array under the optimized polarization state configurations ranges from 51.2% to 62.64%, which is also slightly lower than those of the Uniform states.

It is worth mentioning that, although we only provide examples above for five different desired polarizations, the proposed refined element polarization state optimization strategy can enable the MLPR antenna array to generate a pattern at any desired LPs. This is different from most of the previously reported polarization reconfigurable antenna arrays, which mainly include right-hand CP (RHCP) and left-hand CP (LHCP) [32], LP/CP [33,34], and dual LP [35,36] reconfigurable antenna arrays, as shown in Table 7. These arrays can only achieve a small number of polarization states. To the best of our knowledge, the proposed technique given in this paper is the first to realize an arbitrary LP reconfigurable array that is only fed by equal power dividers. In addition, compared with the arrays reported in Refs. [32–35], the proposed MLPR antenna array can obtain an SLL reduction of 3–4 dB without any excitation amplitude weighting. Moreover, the obtained gain of the proposed array is higher than the reported arrays with 16 elements. An FPGA is adopted to store the optimized polarization state configurations for different LPs. Hence, the MLPR antenna array can be electrically switched to an appropriate polarization state configuration according to the actual requirement of the array polarization.

5. Discussion

As mentioned in Section 2.1, the proposed MLPR antenna array can achieve M^N polarization state configurations, where M is the number of polarization states for each element and N is the number of elements. Hence, the larger the number of element polarization states or the larger the element number is, the more the possible polarization state configurations of the array will be; in that case, the array will be more likely to obtain a better pattern performance in the desired polarization by optimizing the element polarization states. In order to study the influence of using different N and M on the achievable range of SLL and XPL, here we consider several cases with different combinations of N and M. To simplify the discussion, the mutual coupling effect is not taken into consideration. This way, the switching of the polarization state of an array element can be equivalent to rotating the element with a certain angle around its center, as described in Section 2.2. In addition, we choose a rotated ideal dipole antenna pattern to simulate the element pattern at different polarization states. Thus, for the array working at the $\boldsymbol{S}_{1\times N}$ polarization state configuration, the vectorial pattern of its nth element (simulated as a rotated ideal dipole) can be easily derived [46] and is given by the following:

$$\begin{cases} \boldsymbol{E}_{n,\theta}(\theta,\phi) = \dfrac{\cos\left(\frac{\pi}{2}\sin\theta\cos\left(\phi-\varphi_n\right)\right)\cos\theta\cos\left(\phi-\varphi_n\right)}{1-\sin^2\theta\cos^2\left(\phi-\varphi_n\right)}\boldsymbol{e}_\theta \\ \boldsymbol{E}_{n,\phi}(\theta,\phi) = \dfrac{\cos\left(\frac{\pi}{2}\sin\theta\cos\left(\phi-\varphi_n\right)\right)\sin\left(\phi-\varphi_n\right)}{1-\sin^2\theta\cos^2\left(\phi-\varphi_n\right)}\boldsymbol{e}_\phi \end{cases} \tag{15}$$

By substituting Eq. (15) into Eq. (4), the vectorial patterns of such an array can be written as follows:

$$\begin{cases} \boldsymbol{F}_\theta(\theta,\phi;\boldsymbol{S}_{1\times N}) = \sum_{n=1}^{N}\dfrac{\cos\left(\frac{\pi}{2}\sin\theta\cos\left(\phi-\varphi_n\right)\right)\cos\theta\cos\left(\phi-\varphi_n\right)}{1-\sin^2\theta\cos^2\left(\phi-\varphi_n\right)}\mathrm{e}^{\mathrm{j}\beta x_n\cos\phi\sin\theta}\boldsymbol{e}_\theta \\ \boldsymbol{F}_\phi(\theta,\phi;\boldsymbol{S}_{1\times N}) = \sum_{n=1}^{N}\dfrac{\cos\left(\frac{\pi}{2}\sin\theta\cos\left(\phi-\varphi_n\right)\right)\sin\left(\phi-\varphi_n\right)}{1-\sin^2\theta\cos^2\left(\phi-\varphi_n\right)}\mathrm{e}^{\mathrm{j}\beta x_n\cos\phi\sin\theta}\boldsymbol{e}_\phi \end{cases} \tag{16}$$

With the fitness function in Eq. (8), the BGA is used to optimize the polarization state configuration of the array. For all the testing cases, the desired polarization is set to be (90°, 30°) and the optimization goal is set as SLL = −20 dB and XPL = −20 dB. To avoid prematurity of the stochastic optimization algorithm, we perform 200 BGA optimizations for each combination of N and M. Fig. 14 gives the achieved SLL, XPL, and gain of 200 optimizations with M = 4, 6, 8, and 10 for a fixed array element number N = 16. As shown in Fig. 14(a), as M changes from 4 to 8, the obtained SLL is gradually reduced. However, when M is increased from 8 to 10, the SLL of the array is not improved much. The obtained XPL for M = 6 is about 0.8 dB lower than that for M = 4, as shown in Fig. 14(b). When the number of the element polarization states M increases from 6 to 8 or 10, the XPL of the array does not improve much. From Fig. 14(c), it can be seen that, when M is increased from 4 to 8, the obtained gain is increased by about 0.5 dB. In this case, the optimal SLL, XPL, and gain obtained in 200 optimizations are, respectively: −17.04 dB, −17.47 dB, and 14.37 dBi for M = 4; −17.81 dB, −18.46 dB, and 14.72 dBi for M = 6; −18.50 dB, −18.72 dB, and 14.80 dBi for M = 8; and

Table 7
A performance comparison of our proposed array with previously reported polarization reconfigurable antenna arrays.

Ref.	Element antenna type	Number of elements	Feed network	Polarization states	Peak gain (dBi)	Maximum SLL (dB)	Maximum XPL (dB)	Overlapped frequency band (GHz)
[32]	Polarization reconfigurable CP antenna	4 × 4	Single port	RHCP/LHCP	15.50	−11.20	−13.00	2.53–2.57
[33]	Ring slot substrate integrated waveguide cavity patch antenna	2 × 2	Power divider with 90° phase shifters	0° LP, 90° LP, LHCP, RHCP	10.30	−11.00	−20.00	5.30–6.10
[34]	Microstrip antenna	4 × 4	Butler matrix	0° LP, 90° LP, LHCP, RHCP	14.50	−12.00	−16.30	5.00–5.80
[35]	Reconfigurable aperture-fed patch antenna	1 × 4	Equal power divider	+45° LP, −45° LP	13.50	−12.50	−10.00	2.25–2.47
[36]	Dual-polarized slot-ring antenna	2 × 2	10 ports with transmitter and receiver modules	Dual LP	2.40/ 3.10	—	−12.00	1.80–3.70/ 4.50–8.20
This work	MLPR antenna	1 × 16	Equal power divider	Arbitrary LP	17.34–17.53	−16.81–−16.09	−16.03	4.77–5.20

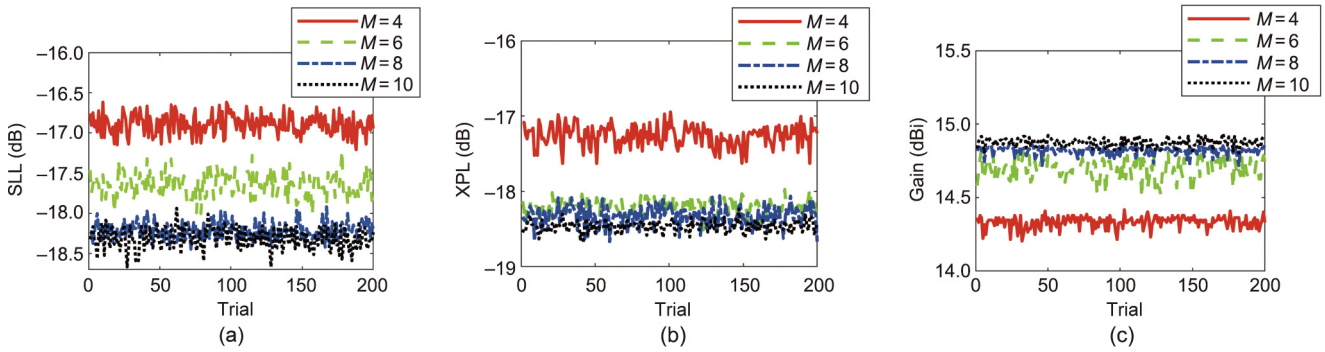

Fig. 14. The obtained (a) SLL, (b) XPL, and (c) gain for M = 4, 6, 8, and 10, with the element number fixed as N = 16. For each M case, 200 BGA optimizations are performed.

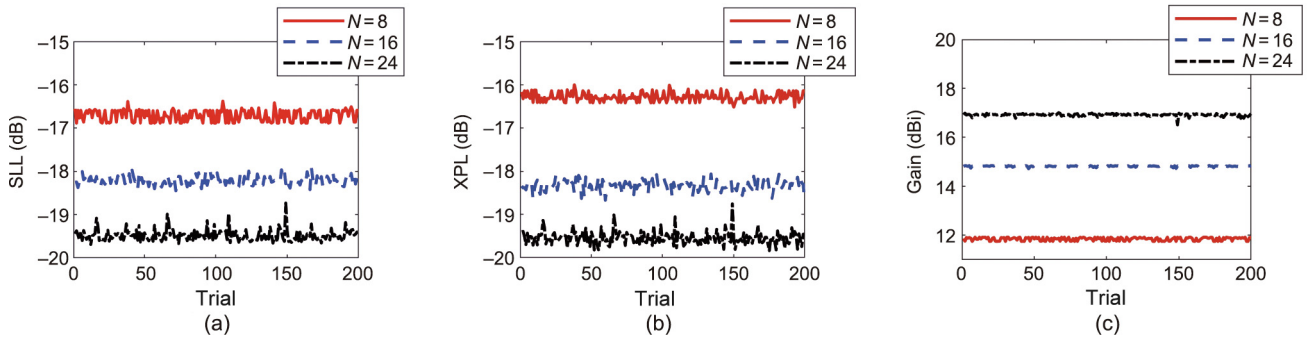

Fig. 15. The obtained (a) SLL, (b) XPL, and (c) gain for N = 8, 16, and 24, with the number of polarization states fixed as M = 8. For each N case, 200 BGA optimizations are performed.

Table 8
The optimal SLL, XPL, and gain obtained in 200 BGA optimizations under various (N, M) combinations.

N	SLL (dB), XPL (dB), gain (dBi)			
	M = 4	M = 6	M = 8	M = 10
8	(−15.03, −16.45, 11.33)	(−16.45, −16.68, 11.81)	(−16.71, −16.34, 11.80)	(−16.54, −17.17, 11.79)
16	(−17.04, −17.47, 14.37)	(−17.81, −18.46, 14.72)	(−18.34, −18.59, 14.80)	(−18.43, −18.62, 14.82)
24	(−18.67, −18.70, 16.37)	(−19.33, −19.64, 16.78)	(−19.53, −19.49, 16.73)	(−19.71, −19.72, 16.75)

−18.43 dB, −18.62 dB, and 14.82 dBi for M = 10. Fig. 15 gives the achieved SLL, XPL, and gain of 200 optimizations with N = 8, 16, and 24 for the fixed element polarization state number M = 8. It can be seen that, when N increases from 8 to 24, the array can achieve increasingly better SLL and XPL. The gain of the array also increases due to the increase of the element number. The optimal SLL, XPL, and gain obtained in 200 optimizations are, respectively: −16.71 dB, −16.34 dB, and 11.80 dBi for N = 8; −18.34 dB, −18.59 dB, and 14.80 dBi for N = 16; and −19.53 dB, −19.49 dB, and 16.73 dBi for N = 24. The optimal SLL, XPL, and gain obtained in 200 optimizations under various combinations of N and M are summarized in Table 8. The ranges of N and M are [8, 16, 24] and [4, 6, 8, 10], respectively. The above results can serve as a reference when choosing the proposed method in this paper.

6. Conclusions

In this work, we have proposed a novel polarization programmable antenna array. The array consists of 16 antenna elements, and each antenna element has eight possible discrete polarization states controlled by an FPGA board. By employing an effective strategy to approximate the vectorial antenna patterns and a BGA for optimizing the element polarization state configuration, the array can generate a pattern with a desired LP and constrained SLL and XPL.

Acknowledgments

This work was supported by the National Natural Science Foundation of China (NSFC) (61871338 and 61721001). The authors would like to thank the editors and reviewers for their valuable advice for the improvement of this paper.

Compliance with ethics guidelines

Dingzhao Chen, Yanhui Liu, Ming Li, Pan Guo, Zhuo Zeng, Jun Hu, and Y. Jay Guo declare that they have no conflict of interest and financial conflicts to disclose.

References

[1] Aghdam SA. Reconfigurable antenna with a diversity filtering band feature utilizing active devices for communication systems. IEEE Trans Antennas Propag 2013;61(10):5223–8.
[2] Trinh LH, Ferrero F, Lizzi L, Staraj R, Ribero JM. Reconfigurable antenna for future spectrum reallocations in 5G communications. IEEE Antennas Wirel Propag Lett 2016;15:1297–300.
[3] Ikram M, Abbas EA, Nguyen-Trong N, Sayidmarie KH, Abbosh A. Integrated frequency-reconfigurable slot antenna and connected slot antenna array for 4G and 5G mobile handsets. IEEE Trans Antennas Propag 2019;67(12):7225–33.
[4] Yang X, Liu Y, Lei H, Jia Y, Zhu P, Zhou Z. A radiation pattern reconfigurable Fabry–Pérot antenna based on liquid metal. IEEE Trans Antennas Propag 2020;68(11):7658–63.

[5] Zhang L, Sun Y, He Y, Wong SW, Mao C, Ge L, et al. A quad-polarization reconfigurable antenna with suppressed cross polarization based on characteristic mode theory. IEEE Trans Antennas Propag 2021;69(2):636–47.
[6] Gao S, Sambell A, Zhong SS. Polarization-agile antennas. IEEE Antennas Propag Mag 2006;48(3):28–37.
[7] Qin PY, Weily AR, Guo YJ, Liang CH. Polarization reconfigurable U-slot patch antenna. IEEE Trans Antennas Propag 2010;58(10):3383–8.
[8] Row JS, Hou MJ. Design of polarization diversity patch antenna based on a compact reconfigurable feeding network. IEEE Trans Antennas Propag 2014;62(10):5349–52.
[9] Tran HH, Nguyen-Trong N, Le TT, Park HC. Wideband and multipolarization reconfigurable crossed bowtie dipole antenna. IEEE Trans Antennas Propag 2017;65(12):6968–75.
[10] Hu J, Hao ZC, Hong W. Design of a wideband quad-polarization reconfigurable patch antenna array using a stacked structure. IEEE Trans Antennas Propag 2017;65(6):3014–23.
[11] Wu F, Luk KM. A reconfigurable magneto–electric dipole antenna using bent cross-dipole feed for polarization diversity. IEEE Antennas Wirel Propag Lett 2017;16:412–5.
[12] Yang W, Che W, Jin H, Feng W, Xue Q. A polarization-reconfigurable dipole antenna using polarization rotation AMC structure. IEEE Trans Antennas Propag 2015;63(12):5305–15.
[13] Cui Y, Qi C, Li R. A low-profile broadband quad-polarization reconfigurable omnidirectional antenna. IEEE Trans Antennas Propag 2019;67(6):4178–83.
[14] Tran HH, Park HC. Wideband reconfigurable antenna with simple biasing circuit and tri-polarization diversity. IEEE Antennas Wirel Propag Lett 2019;18(10):2001–5.
[15] Liu P, Jiang W, Sun S, Xi Y, Gong S. Broadband and low-profile penta-polarization reconfigurable metamaterial antenna. IEEE Access 2020;8:21823–31.
[16] Tran HH, Nguyen-Trong N, Le TT, Abbosh AM, Park HC. Low-profile wideband high-gain reconfigurable antenna with quad-polarization diversity. IEEE Trans Antennas Propag 2018;66(7):3741–6.
[17] Wong H, Lin W, Huitema L, Arnaud E. Multi-polarization reconfigurable antenna for wireless biomedical system. IEEE Trans Biomed Circuits Syst 2017;11(3):652–60.
[18] Nguyen-Trong N, Piotrowski A, Hall L, Fumeaux C. A frequency- and polarization-reconfigurable circular cavity antenna. IEEE Antennas Wirel Propag Lett 2017;16:999–1002.
[19] Chang LH, Lai WC, Cheng JC, Hsue CW. A symmetrical reconfigurable multipolarization circular patch antenna. IEEE Antennas Wirel Propag Lett 2014;13:87–90.
[20] Yang Y, Zhu X. A wideband reconfigurable antenna with 360° beam steering for 802.11ac WLAN applications. IEEE Trans Antennas Propag 2018;66(2):600–8.
[21] Gu H, Wang J, Ge L, Sim CYD. A new quadri-polarization reconfigurable circular patch antenna. IEEE Access 2016;4:4646–51.
[22] Chen SL, Wei F, Qin PY, Guo YJ, Chen X. A multi-linear polarization reconfigurable unidirectional patch antenna. IEEE Trans Antennas Propag 2017;65(8):4299–304.
[23] Lin W, Wong H. Multipolarization-reconfigurable circular patch antenna with L-shaped probes. IEEE Antennas Wirel Propag Lett 2017;16:1549–52.
[24] Sano M, Higaki M. A linearly polarized patch antenna with a continuously reconfigurable polarization plane. IEEE Trans Antennas Propag 2019;67(8):5678–83.
[25] Xu C, Wang Y, Wu J, Wang Z. Parasitic circular patch antenna with continuously tunable linear polarization using liquid metal alloy. Microw Opt Technol Lett 2019;61(3):727–33.
[26] Tanaka M. Polarization-changeable phased array. In: Proceedings of IEEE Antennas and Propagation Society International Symposium; 1999 Jul 11–16; Orlando, FL, USA. IEEE; 1999. p. 2322–5.
[27] Li J, Compton RT. Angle and polarization estimation using ESPRIT with a polarization sensitive array. IEEE Trans Antennas Propag 1991;39(9):1376–83.
[28] Haskins PM, Dahele JS. Polarisation agile active microstrip patch arrays. Electron Lett 1996;32(6):509–11.
[29] Li W, Gao S, Cai Y, Luo Q, Sobhy M, Wei G, et al. Polarization-reconfigurable circularly polarized planar antenna using switchable polarizer. IEEE Trans Antennas Propag 2017;65(9):4470–7.
[30] Slomian I, Wincza K, Gruszczynski S. Series-fed microstrip antenna lattice with switched polarization utilizing butler matrix. IEEE Trans Antennas Propag 2014;62(1):145–52.
[31] Lin W, Wong H. Polarization reconfigurable aperture-fed patch antenna and array. IEEE Access 2016;4:1510–7.
[32] Shirazi M, Li T, Huang J, Gong X. A reconfigurable dual-polarization slot-ring antenna element with wide bandwidth for array applications. IEEE Trans Antennas Propag 2018;66(11):5943–54.
[33] Haupt RL, Werner DH. Genetic algorithms in electromagnetics. Hoboken: John Wiley & Sons; 2007.
[34] Jin N, Rahmat-Samii Y. Advances in particle swarm optimization for antenna designs: real-number, binary, single-objective and multiobjective implementations. IEEE Trans Antennas Propag 2007;55(3):556–67.
[35] Keizer WPMN. Fast low-sidelobe synthesis for large planar array antennas utilizing successive fast Fourier transforms of the array factor. IEEE Trans Antennas Propag 2007;55(3):715–22.
[36] Lebret H, Boyd S. Antenna array pattern synthesis via convex optimization. IEEE Trans Signal Process 1997;45(3):526–32.
[37] Haupt RL, Aten DW. Low sidelobe arrays via dipole rotation. IEEE Trans Antennas Propag 2009;57(5):1575–9.
[38] Li M, Liu Y, Chen SL, Qin PY, Guo YJ. Low sidelobe synthesis of dipole arrays by element orientation selection using binary coded genetic algorithm. In: Proceedings of 2017 11th European Conference on Antennas and Propagation (EUCAP); 2017 Mar 19–24; Paris, France. IEEE; 2017. p. 2838–40.
[39] Echeveste JI, Rubio J, Aza MAGD, Craeye C. Pattern synthesis of coupled antenna arrays via element rotation. IEEE Antennas Wirel Propag Lett 2017;16:1707–10.
[40] Li M, Liu Y, Guo YJ. Shaped power pattern synthesis of a linear dipole array by element rotation and phase optimization using dynamic differential evolution. IEEE Antennas Wirel Propag Lett 2018;17(4):697–701.
[41] Liu F, Liu Y, Xu KD, Ban YL, Liu QH, Guo YJ. Synthesizing uniform amplitude sparse dipole arrays with shaped patterns by joint optimization of element positions, rotations and phases. IEEE Trans Antennas Propag 2019;67(9):6017–28.
[42] Ludwig A. The definition of cross polarization. IEEE Trans Antennas Propag 1973;21(1):116–9.
[43] Pampara G, Engelbrecht AP, Franken N. In: Binary differential evolution. Vancouver, BC, Canada: IEEE; 2006. p. 1873–9.
[44] infineon.com [Internet]. Munich: Infineon Technologies AG; c1999–2022 [cited 2021 Sep 3]. Available from: https://www.infineon.com/.
[45] china-fenghua [Internet]. Zhaoqing: Guangdong Fenghua Advanced Technology Holding Co., Ltd.; c2017 [cited 2021 Sep 3]. Available from: http://www.china-fenghua.com/.
[46] Stutzman WL, Thiele GA. Antenna theory and design. 2nd ed. Hoboken: John Wiley & Sons; 1998.